Croatian Society for Materials Protection

Metalurgija/Metallurgy

Vol. 66 No. 1 / 2027

Replacement of an Assembled Tamping Pick for an Integral Tamping Pick

Yue Cui[1], Liyuan Wang[2,*], Huigang Wang[1], Xiangbin Yang[1], Shidong Shi[1], and Huijie Han[3]

https://doi.org/10.64486/m.66.1.8

[1] Key Lab of Intelligent Equipment Digital Design and Process Simulation, Tangshan University, Tangshan 063000, China
[2] Department of Intelligent Manufacturing, Tangshan Vocational College of Science and Technology, Tangshan 063001, China
[3] Tangshan Metallurgical Saw Blade Co., Ltd., Tangshan 063020, China
* Correspondence: wly17713170132@163.com

Type of the Paper: Article
Received: January 16, 2026
Accepted: May 29, 2026

Abstract: Aimed at optimizing resource utilization, this study leverages finite element analysis (FEA) to compare integral and assembled tamping picks—both are pivotal components in railway ballast tamping machines prone to wear. Traditional integral picks, cast/forged with embedded wear-resistant alloys, suffer from material waste, as they compel full replacement upon head wear. The FEA involved static and modal analyses, where the former revealed that the assembled picks exhibited a maximum equivalent stress 27.5 MPa higher than the integral ones, free from any significant stress concentration. The integral picks concentrated stress on upper/lower surfaces, incurring the under-utilization of mid-section material. The modal analysis compared resonance in the first 10 vibration modes. For the integral picks, the 10th mode demonstrated a maximum amplitude (34.2 mm, 6815.5 Hz) localized at the head. The assembled picks possessed higher amplitudes in the 3rd (69.3 mm), 4th (69.4 mm), 8th (65.6 mm), and 9th (64.6 mm) modes—all on the pole. As manifested by the results, the integral picks' material waste and stress inefficiency are curtailed by the assembled designs. Notwithstanding their slightly higher static stress, the assembled picks show dynamic behavior (higher amplitudes on the pole vs. head) that aligns better with wear patterns, so that the localized replacement is feasible. Consequently, the assembled tamping picks, supported by FEA results, present a preliminary numerical analysis for more economical solution for railway maintenance.

Keywords: tamping pick, integral, assembled, finite element method, static analysis, modal analysis

1. Introduction

The booming railway transportation in China spawns rocketing demand for railway maintenance, which gives rise to the increasingly stringent requirements on maintenance equipment, particularly for large-scale road maintenance machinery. A compactor can underpin the stability of the railway track by compressing the ballast of the track bed. As an indispensable component of the compaction vehicle, the tamping pick collides and compacts with the ballast during operation, which incurs severe wear and tear. In view of this, investigating the structural types of tamping picks is thereby of enormous necessity.

Liu et al. summarized the vibration excitation of tamping machinery, and pioneered an innovative electro-hydraulic excitation strategy for tamping devices [1]. Based on the structural traits of the tamping pick part, Wang Jie et al. merged the Kriging interpolation idea and optimal space-filling design sampling, so as to construct an initial agent model applicable to mechanical structural optimization design [2]. Qian et al. launched a simulation model for the manual tamping device-ballast bed system relying on a coupling modeling approach that fuses discrete element and multi-body dynamics [3]. Wang et al. simulated the state quantity curves and the motion characteristic curves of the tamping pick impact system [4]. Xiao Wen-jian et al. refined the structural form of the tamping pick in light of modal analysis [5]. Revolving around the tamping machine, Li analyzed the tamping performance and structural optimization of the hammer lifting mechanism [6]. Sun and Center delved into the dynamic traits, and plotted the life curve of the tamping hammer [7]. As demonstrated by Liu and Gong, a novel tamping machine, which hinges on hydraulic vibration with load sensing and stepless regulation of operating parameter, can mitigate the wear on tamping bar through forced vibration [8]. Zhang et al. measured the vibration force of the tamping pick, then tuned and reinforced the weak points of the tamping machine [9]. Wang adjusted the compaction device of the 08/09-32 type tamping vehicle, which exerted an augmented compaction effect [10]. An attrition testing machine was developed by Wen et al. for railway tamping pickaxes, attaining adjustable vibration frequency, plentiful stone material types, and distinguishable pickaxe materials [11]. According to Shang et al., the microstructure and properties of the alloy manifested superior advantages over those of as forged tamping picks (normalized) after an optimized quenching–tempering process [12]. Xiao dissected the vibration mode of the internal combustion tamping pick by examining its harmonic response to assess the effectiveness of vibration reduction measures [13]. Rodrigues, P and Teixeira, P.F propounded a multiple linear regression model to predict the post-tamping defect level [14]. Raghavendra, H.N. exploited an array of lateral loading tests to establish an optimal taper angle and segments for both tapered and step-tapered piles [15]. Morariu-Gligor put forth a mechanical and mathematical model for a tamping pick, which was applicable to construction walls [16]. Offenbacher et al. elucidated the relation between the compaction during tamping and the track behavior [17]. A side tamping strategy was introduced by Przybylowicz et al. as an alternative, ballast saving, and sleeper form independent ballast tamping technique [18]. Bakhtiary et al. expounded on an opportunistic preventive maintenance policy to schedule tamping interventions [19]. Morariu-gligor created a mechanical and a mathematical model, aiming at exploring the dynamical behavior of a tamping rammer [20]. Offenbacher et al. gauged a plurality of parameters during each tamping process using a tamping machine equipped with sensors [21]. Typically fabricated as a whole, the tamping picks are distributed at both ends of the tamping vehicle.

The research probes into multi-dimensional tamping optimizations. Concretely, the high-frequency amplitude bias is resolved by electro-hydraulic excitation via stepper motor-driven valves and hydraulic cylinders, with load-sensing/stepless regulation as trends. Manual tamping diminishes ballast stiffness while enhancing contact uniformity and mitigating sleeper-edge particle distinction. Lateral tamping intensifies sleeper-end compaction and residual stress, with twice the wave propagation velocity, despite the vertical methods excelling in settlement resistance. Special structures shrink maintenance cycles by 60 %, and the defect morphology inflict impact on recovery. The data integration links onboard tamping metrics with track geometry by means of spatial synchronization. An opportunistic maintenance framework involving genetic algorithms cuts the mechanical costs by 46 % through OMT optimization, revealing the more drastic negative impact of inefficient tamping. All the efforts converge on reinforcing stability at minimal lifecycle costs. The tamping picks are driven downward by the hydraulic device, then inserted into the track bed during the operation. The gap between the stone ballast particles is narrowed with the vibration of the tamping picks, which further stabilizes the track ballast slag (Figure 1).

https://doi.org/10.64486/m.66.1.8

Figure 1. On-site photos of the tamping picks

The integral tamping pick comprises a pick body and a pick head. Amid the operation, the tamping pick manufactured through integral forging confront two drawbacks: Firstly, the entire tamping pick has to be scrapped once the pick head at a prohibitive forging cost breaks during the tamping operation. Secondly, the brazing takes part in the preparation of the tamping pick, for the sake of wrapping the hard alloy around the pick. Although such a structure elongates the service life, substituting the pick after the hard alloy scrapping is extremely cumbersome.

In this work, the stress distribution characteristics are analyzed and compared for two types of tamping picks: integral and assembled structures, with the purpose of replacing integral tamping picks with assembled ones. It also lays a theoretical foundation for fabricating assembled structures, and alleviates the reliance on costly experimental manufacturing and testing procedures.

2. Finite Element Calculation Model

The models of the integral structure (Figure 2a) and assembled structure (Figure 2b) were constructed based on the configuration of the tamping pick, where the assembled structure consists of a tamping pick head, a pick body, and a pick pole. The integral structure subject to analysis was made of wear-resistant material (GCr15). Comparatively, in the assembled structure, the study uses GCr15 for the tamping pick head, and conventional 40CrNiMo steel for the body and pole. GCr15 bearing steel was a high-carbon chromium alloy steel that forms a martensitic microstructure with fine dispersed carbides (Fe3C) after standard quenching and tempering heat treatment (830 ℃ – 850 ℃ oil quenching + 160 ℃ – 180 ℃ low-temperature tempering), which endows it with high hardness (60 HRC–64 HRC), excellent wear resistance and contact fatigue strength—these properties were critical for the tamping pick head that experiences direct impact and abrasive wear against railway ballast particles [22–23]. 40CrNiMo alloy steel was a low-alloy high-strength steel that forms a tempered bainite microstructure after quenching and high-temperature tempering (850 ℃ water quenching + 550 ℃ – 600 ℃ tempering), which had a small ductile damage under specific process conditions during the high-temperature cross wedge rolling for the manufacturing of the high-speed railway axles [24]. The yield strength of 40CrNiMo steel increased from 1153 MPa to 1323 MPa by refinement hardening and dislocation hardening [25], which was ideal for the pick body and pole that undergo dynamic bending and twisting loads without direct ballast contact. The interface bonding between GCr15 pick head and 40CrNiMo pick pole in the assembled structure was optimized through mechanical interlocking, which ensures effective stress transfer and structural stability under dynamic impact loading conditions.

The material properties used in the finite element model are summarized in Table 1.

https://doi.org/10.64486/m.66.1.8

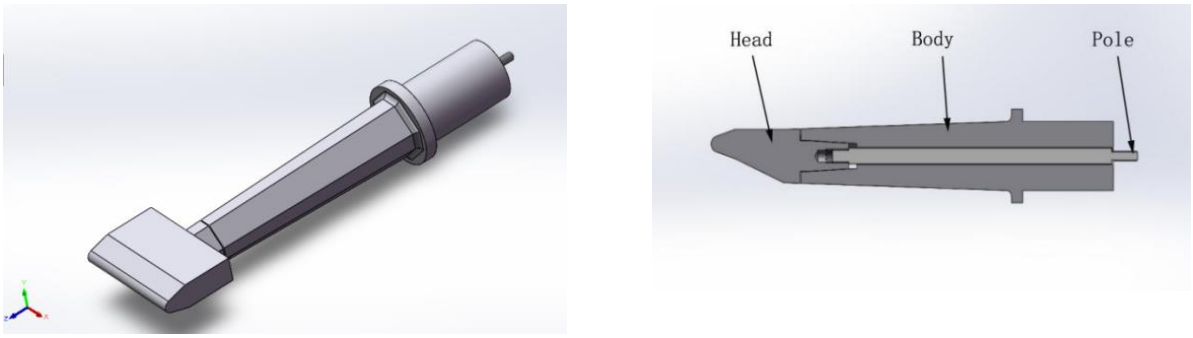

a. Integral tamping pick **b.** Assembled tamping pick (section)

Figure 2. Two types of tamping picks with different structures

Table 1. Parameters of Materials

Material	Elastic modulus / MPa	Poisson's ratio	Density / kg/m^3
GCr15	2.19×10^5	0.300	7.83×10^3
40CrNiMo	2.09×10^5	0.295	7.87×10^3

Grid refinement was executed to the integral tamping pick model, with a C3D8 linear hexahedral element grid type assigned, which acquired 95 311 elements in total (Figure 3a). The tied contact formulation was implemented with respect to the joint interface between the pick head, body and pole (Figure 3b). This optimized contact modeling efficiency, shortened computational time, and stabilized numerical convergence. For the assembled tamping pick model, the C3D8 linear hexahedral element type was also involved for mesh generation, totally producing 105 987 elements.

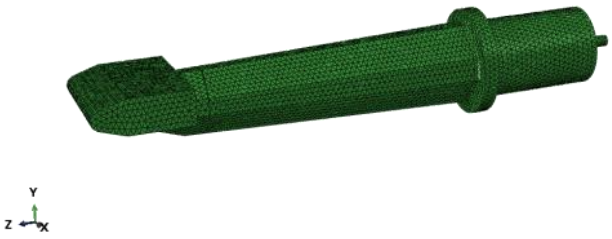

a. Grid division of the integral tamping pick

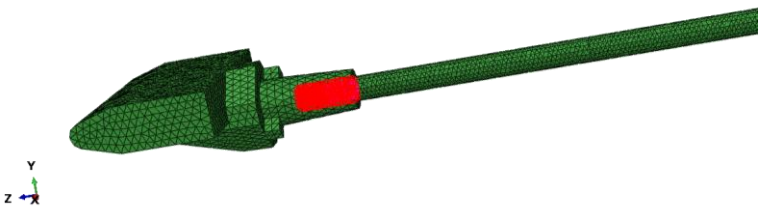

b. Processing of the connection position between the assembled head and the pole

Figure 3. Grid divisions of tamping picks with different structures

The proximal end of the tamping pick was rigidly constrained, and a 30 000 N impact force was imposed to the tool head, so as to simulate the tamping pick's working state. The 30 kN static impact force was derived from the on-site operational statistical data of the 08/09-32 type tamping vehicle, which was the average value of the actual impact force between tamping picks and ballast in normal continuous operation. Field test data provided by China Railway Beijing Bureau Group Co., Ltd. verifies that this static force was a reasonable engineering simplification for the average static equivalent of dynamic impact loads in FEA analysis of railway

https://doi.org/10.64486/m.66.1.8

tamping components [11]. The rigid constraint of the tamping pick proximal end was consistent with the actual clamping mode of the hydraulic chuck of the tamping vehicle, which was a widely accepted simplification method in the FEA simulation of railway engineering mechanical components. It was observed that the vibration frequency was 35 Hz, and the vibration amplitude was 3.0 mm–6.6 mm.

3. Static Stress Analysis

After pre-processing the model, the solving module (Job) in ABAQUS was leveraged to compute the equivalent stress distribution as shown in Figure 4.

Figure 4 illustrates the discrepancy of maximum stress location between the two tamping picks. The maximum stress of the integral tamping pick occurs at the handle of the tamping pick (Figure 4a), with a maximum stress of 264.7 MPa. The maximum stress of the assembled tamping pick arises at the head-pole connection (Figure 4b), alongside a maximum stress of 292.2 MPa.

The maximum stress values of the two structures differ by 27.5 MPa, with no notable stress concentration spotted. During the operation of the integral tamping pick, the stress is predominantly distributed on the upper and lower surfaces of the pick body, and the material in the middle position is not thoroughly exploited. The assembled structure transfers the location of the maximum stress to the head-pole connection, and the stress is distributed from the inside out. In light of static analysis, it is viable to structurally decompose the integral tamping pick into pick head, pick pole, and pick body.

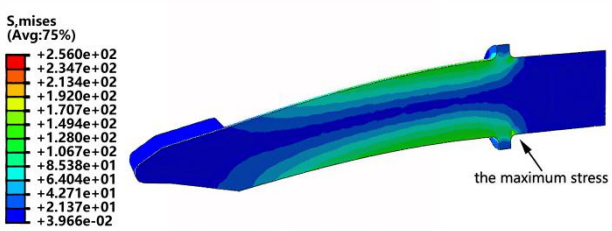

a. Integral equivalent stress distribution (section)

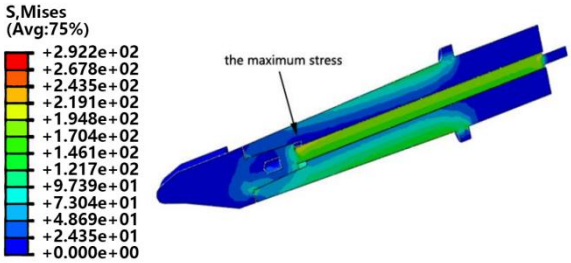

b. Assembled equivalent stress distribution (section)

Figure 4. Equivalent stress distributions of tamping picks with different structures

4. Modal Analysis

Modal analysis represents a fundamental method for deciphering vibration, which is required for both of the two structures, because the tamping pick must be able to compact ballast through induced vibrations during operational cycles.

4.1. Modal Analysis of the Integral Tamping Pick

A holistic modal analysis was undertaken to garner solution variables predicated on the integral tamping pick model. Post-processing visualization extracted the first ten vibration modes as presented in Figure 5a–5j. Key characteristics of each mode are delineated as below:

https://doi.org/10.64486/m.66.1.8

First-order mode: The front end of the tamping pick swung along the X-axis direction in the XOZ plane, with a maximum amplitude of 21.1 mm.

Second-order mode: The front end of the tamping pick swung along the Y-axis direction in the YOZ plane, with a maximum amplitude of 20.7 mm.

Third-order mode: The tamping pick rotated along the Z-axis with a maximum amplitude of 32.6 mm.

Fourth-order mode: The entire tamping pick twisted along the Y-axis direction, with a maximum amplitude of 24.3 mm.

Fifth-order mode: The tamping pick rotated along the Z-axis, with a maximum amplitude of 20.8 mm.

Sixth-order mode: The front end of the tamping pick moved along the Z-axis direction in the YOZ plane, with a maximum amplitude of 16.1 mm.

Seventh-order mode: The overall tamping pick twisted left and right in an S-shape along the Z-axis in the XOZ plane, with a maximum amplitude of 21.0 mm.

Eighth-order mode: The overall tamping pick twisted up and down in an S-shape along the Z-axis in YOZ, with a maximum amplitude of 23.9 mm.

Ninth-order mode: The pick body follows a tendency to expand and increase, and the pick rotated along the Z-axis, with a maximum amplitude of 24.4 mm.

Tenth-order mode: The tamping pick twisted as a whole in a W-shape along the Z-axis in the YOZ plane, with a maximum amplitude of 34.2 mm.

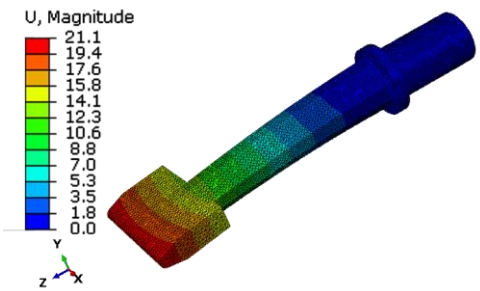

a. First-order mode

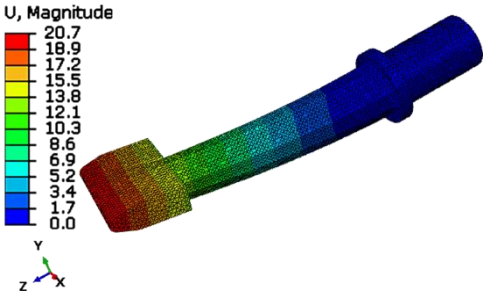

b. Second-order mode

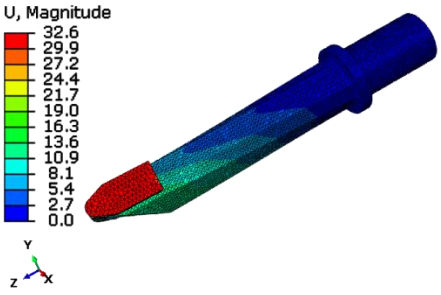

c. Third-order mode

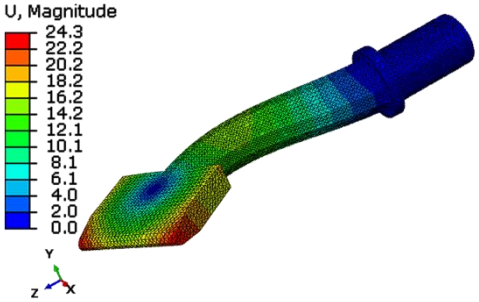

d. Fourth-order mode

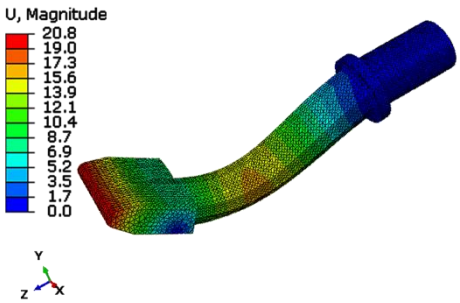

e. Fifth-order mode

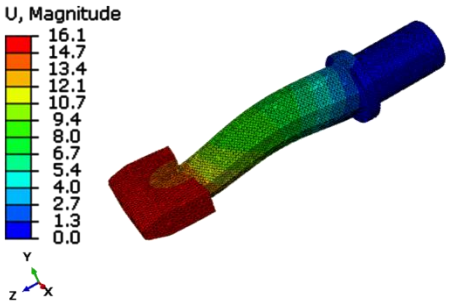

f. Sixth-order mode

https://doi.org/10.64486/m.66.1.8

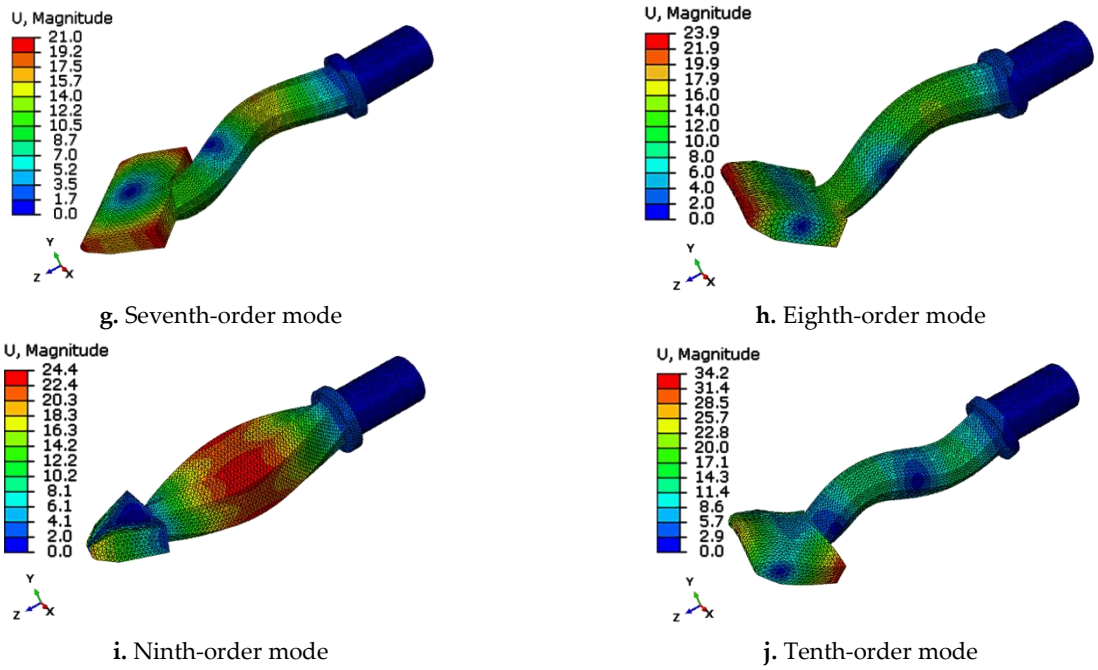

g. Seventh-order mode **h.** Eighth-order mode

i. Ninth-order mode **j.** Tenth-order mode

Figure 5. Ten order modal analysis of the integral tamping pick

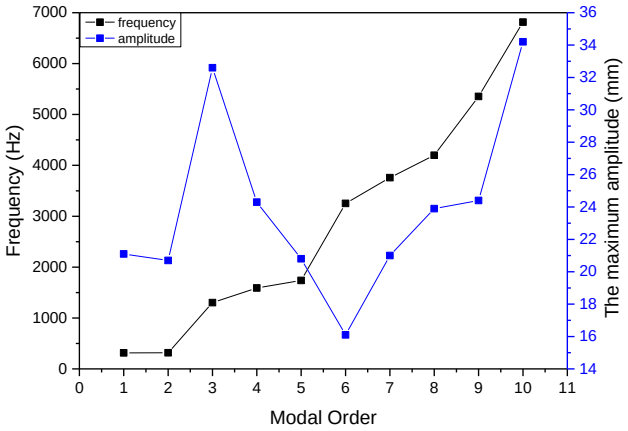

Figure 6. Modal analysis of the first ten frequencies and maximum amplitude of the integral tamping pick

According to the analysis of the first ten vibration modes of the integral tamping pick (Figure 6), the maximum vibration amplitude emerged at the 10th-order mode, measuring 34.2 mm at 6815.5 Hz, situated at the top of the tamping pick head. The vibration was basically composite, involving bending and twisting deformation. The amplitude of the tamping pick head was larger than the other parts, rendering it the most susceptible to damage.

4.2. Modal Analysis of the Assembled Tamping Pick

This study implemented a modal analysis on the tamping pick of the assembled structure, and derived the first ten modes as presented in Figure 7a–7j.

https://doi.org/10.64486/m.66.1.8

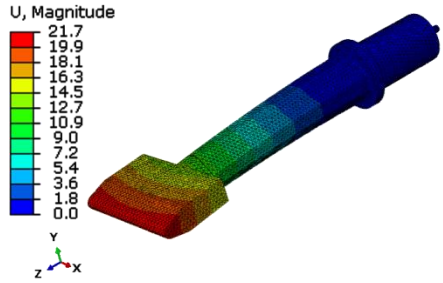

a. First-order mode

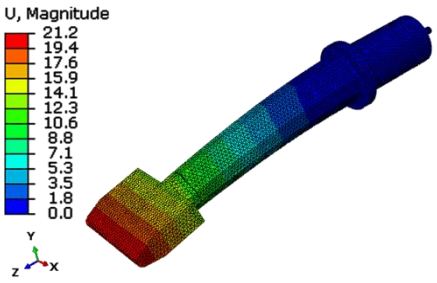

b. Second-order mode

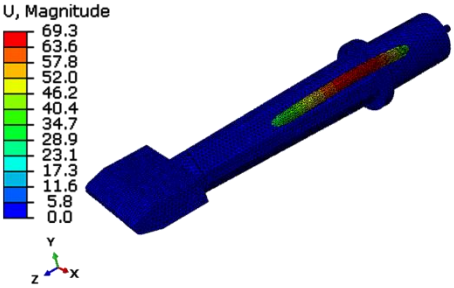

c. Third-order mode

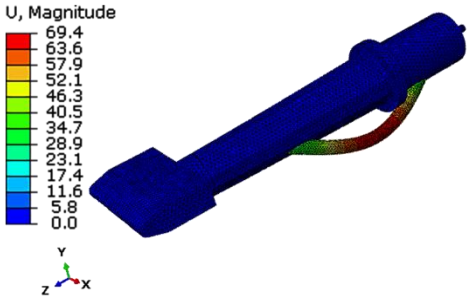

d. Fourth-order mode

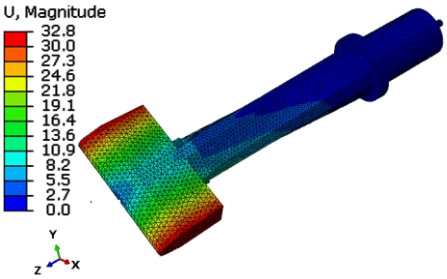

e. Fifth-order mode

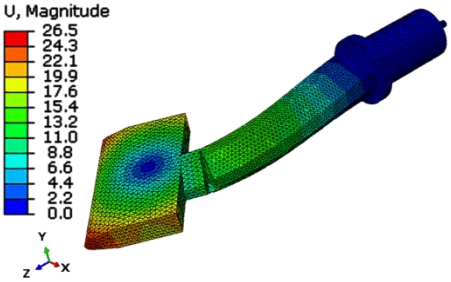

f. Sixth-order mode

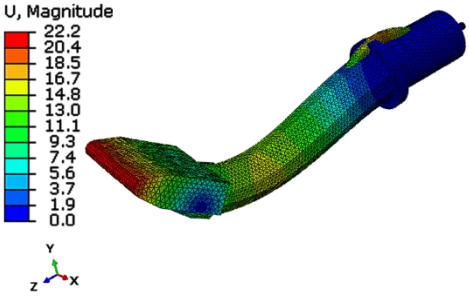

g. Seventh-order mode

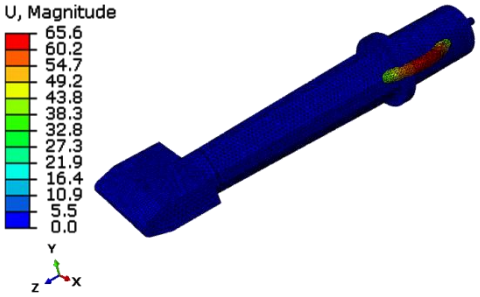

h. Eighth-order mode

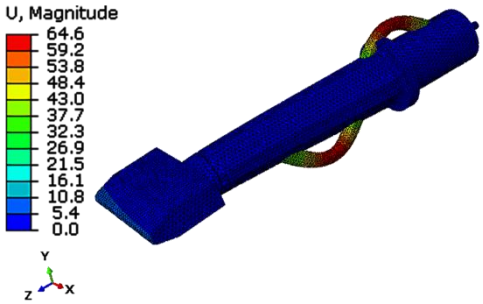

i. Ninth-order mode

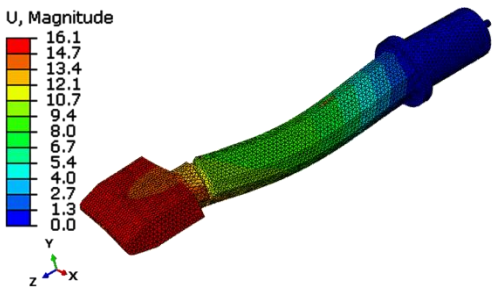

j. Tenth-order mode

Figure 7. Ten order modal analysis of the assembled tamping pick

https://doi.org/10.64486/m.66.1.8

The modal analysis of the assembled tamping pick reveals prominent vibration characteristics across the first ten modes:

First-order mode: The front end of the tamping pick swung along the X-axis direction in the XOZ plane, with a maximum amplitude of 21.7 mm.

Second-order mode: The front end of the tamping pick swung along the Y-axis direction in the YOZ plane, with a maximum amplitude of 21.2 mm.

Third-order mode: The middle part of the pick pole vibrated at a 45° angle along the positive X-axis and Y-axis directions in the XOY plane, with a maximum amplitude of 69.3 mm.

Fourth-order mode: The middle part of the pick pole vibrated at a 45° angle along the positive and negative directions of the X-axis and Y-axis in the XOY plane, with a maximum amplitude of 69.4 mm.

Fifth-order mode: The tamping pick rotated along the Z-axis, with a maximum amplitude of 32.8 mm.

Sixth-order mode: The entire tamping pick twisted along the Y-axis direction, with a maximum amplitude of 26.5 mm.

Seventh-order mode: The assembly exhibits S-shaped deformation in the YOZ plane, with 22.2 mm of out-of-plane warping along the Y-axis.

Eighth-order mode: The pick pole twisted in an S-shape along the X-axis direction in the XOZ plane, with a maximum amplitude of 65.6 mm.

Ninth-order mode: The pick rod twisted in an S-shape along the Y-axis direction in the YOZ plane, with a maximum amplitude of 64.6 mm.

Tenth-order mode: The tamping pick moved along the positive Z-axis direction in YOZ and twisted in an S-shape in the Y-axis direction, with a maximum amplitude of 16.1 mm.

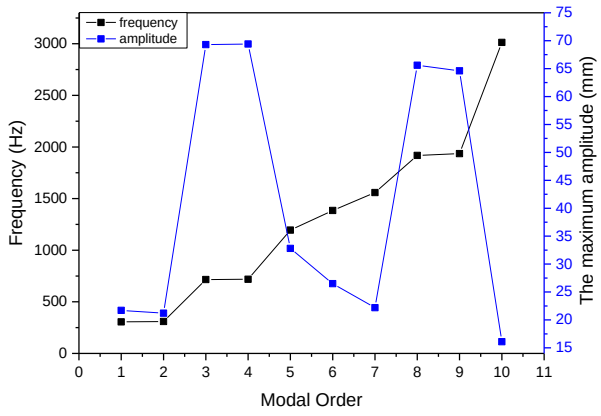

Figure 8. Modal analysis of the first ten frequencies and maximum amplitude of the assembled tamping pick

After analyzing the first ten vibration modes of the assembled tamping pick (Figure 8), the maximum amplitude was observed in the third, fourth, eighth, and ninth orders, with values of 69.3, 69.4, 65.6, and 64.6 mm, respectively—all of which were localized at the tamping pick pole. The primary mode of vibration was analogous to the integral tamping pick configuration, which was a composite vibration involving bending and twisting deformation. The tamping pick pole showed a larger amplitude than the other parts, conveying that fatigue failure exerts the most influence on this region.

5. Conclusion and Discussion

In this study, two types of tamping picks were subject to the finite element analysis, and the chief conclusions were elucidated as below:

1) By comparing the static analysis of the two structures, a minor maximum stress difference of 27.5 MPa was observed between the assembled structure and the integral structure. The assembled structure

https://doi.org/10.64486/m.66.1.8

transferred the stress generated to the pick pole, ensuring highly uniform stress distribution, while the assembled structure exhibited a higher utilization rate of structural materials.

2) The dynamic analysis corroborated that the resonance frequency of the two structures was beyond the normal operating frequency range. The integral structure can be replaced after the rigidity of the assembled tamping pick pole was strengthened, and the assembled structure was superior to the integral structure.

3) In the later practical use of the two tamping picks, the assembled structure demonstrated a longer service life than the integral structure. This affirms the technical feasibility of substituting the integral tamping pick with the assembled tamping pick.

In practical railway maintenance engineering, the integral tamping pick was typically scrapped when the head wear reaches 10 mm with an average actual service life of approximately 300 operating hours; while the assembled tamping pick only requires local replacement of the worn pick head (the replacement time is less than 1 hour) and the pick body/pole can continue to operate. This modular design significantly improves the overall service efficiency of the tamping pick and reduces material waste. Overall, this study presents a preliminary numerical analysis of substituting the integral tamping pick with the assembled tamping pick in engineering practice.

Future efforts will focus on the contact analysis between tamping pick and slag, as well as the contact fatigue and wear calculations to optimize the structure of the assembled tamping pick.

Acknowledgments

This research was funded by the Development Funds of the Central Government for Local Science and Technology (No. 236Z1701G).

Reference

[1] Y. Liu, G. Gong, and C. Min, "Present status and prospect of tamping device exciting technology," J. Mech. Eng., vol. 49, no. 16, pp. 138–146, 2013, https://doi.org/10.3901/JME.2013.16.138

[2] J. Wang, T. Wang, and S. Ye, "Optimization of the railway tamping pick based on modified kriging model," Chin. J. *Constr. Mach*., vol. 19, no. 4, pp. 331–336, 2021, https://doi.org/10.15999/j.cnki.311926.2021.04.009

[3] Z. Qian, H. Xiao, and Z. Zhang, "Establishment and mechanical performance analysis of manual tamping operation model for ballast bed," *J. Cent. South Univ. (Sci. Technol.)*, vol. 55, no. 3, pp. 1241–1251, 2024, https://doi.org/10.11817/j.issn.1672-7207.2024.03.015

[4] T. Wang, H. Liu, and L. Wang, "Simulation and analysis for impact characteristics of internal combustion tamping pick," *Mach. Des. Manuf*., no. 7, pp. 19–23, 2021, https://doi.org/10.19356/j.cnki.1001-3997.2021.07.005

[5] W. Xiao, Z. Ni, and J. Wu, "Modal analysis and optimization of tamping pick handheld device based on ANSYS," *Sci. Technol. Innov*., no. 3, pp. 119–120, 2018

[6] Z. Li, "Analysis of the Tamping Performance and Structural Optimization of the Hammer Lifting Device of the Coal Cake Tamping Machine," Dalian Jiaotong Univ., Dalian, China, 2023, https://doi.org/10.26990/d.cnki.gsltc.2023.000420

[7] N. X. Sun and T. Center, "Dynamic Analysis and Study of Eight Tamping Hammer Unit of 6.25m Tamping Machine," *Mech. Eng. Autom*., no. 3, pp. 95–96+98, 2017, https://link.cnki.net/urlid/14.1319.TH.20170503.1534.078

[8] Y. Liu and G. Gong, "Kinetic analysis of new tamping arm," *J. Cent. South Univ. (Sci. Technol.)*, vol. 46, no. 9, pp. 3211–3216, 2015, https://doi.org/10.11817/j.issn.1672-7207.2015.09.007

[9] M. Zhang, Y. Li, and L. Sun, "Research on evaluation method of tamping picks exciting force," *Railw. Eng*., no. 9, pp. 114–116, 2013, https://doi.org/10.3969/j.issn.1003-1995.2013.09.36

[10] Y. Wang, "Reformation design on type 08/09–32 tamping unit," *Railw. Eng*., no. 2, pp. 113–115, 2014, https://doi.org/10.3969/j.issn.1003-1995.2014.02.36

[11] Y. Wen, X. Huang, and W. Zhong, "Attrition Testing Machine about the Railway Pickaxe of Tamping Pick," *Mach. Des. Res*., vol. 35, no. 3, pp. 193–198, 2019, https://doi.org/10.13952/j.cnki.jofmdr.a4927

[12] X. Shang, J. Li, and S. Yuan, "Effects of Quenching-Tempering Process on Microstructures and Mechanical Properties of Tamping Tine Made of 35CrMo Steel," *Hot Work. Technol*., no. 1, pp. 1–5, 2023, https://doi.org/10.14158/j.cnki.1001-3814.20212055

[13] W. Xiao, "Research on Vibration Analysis and Vibration Reduction Design of Internal Combustion Tamping Pick," Hunan Univ. Technol., Changsha, China, 2018

[14] P. Rodrigues and P. F. Teixeira, "Modelling tamping effectiveness for track geometry longitudinal levelling defects," *Proc. Inst. Mech. Eng., Part F: J. Rail Rapid Transit*, vol. 238, no. 6, pp. 662–674, 2024, https://doi.org/10.1177/09544097231181576

[15] H. N. Raghavendra, P. Kappadi, and H. Likhitha, "The Behavior of Tapered and Step-Tapered Piles under Lateral Load," *Eng. Lett*., vol. 33, no. 3, pp. 530–544, 2025, https://doi.org/10.5281/zenodo.10674563

[16] R. M. Morariu-Gligor, "Mathematical and Mechanical Model of a Tamping Rammer for Making Rammed Earth Walls," Adv. Serv. Ind. Robot.: RAAD, *Mech. Mach. Sci*., vol. 157, pp. 389–398, 2024, https://doi.org/10.1007/978-3-031-46231-5_26

[17] S. Offenbacher, C. Koczwara, and M. Landgraf, "A Methodology Linking Tamping Processes and Railway Track Behaviour," *Applied Sciences*, vol. 13, no. 4, article 2137, 2023, https://doi.org/10.3390/app13042137

[18] M. Przybylowicz, M. Sysyn, and U. Gerber, "Comparison of the effects and efficiency of vertical and side tamping methods for ballasted railway tracks," *Constr. Build. Mater*., vol. 314, p. 124156, 2022, https://doi.org/10.1016/j.conbuildmat.2021.124156

[19] A. Bakhtiary, J. A. Zakeri, and S. Mohammadzadeh, "An opportunistic preventive maintenance policy for tamping scheduling of railway tracks," *Int. J. Rail Transp*., vol. 9, no. 1, pp. 1–22, 2021, https://doi.org/10.1080/23248378.2019.1696463

[20] R. M. Morariu-Gligor, "The Study of the Dynamic Behavior for a Tamping Rammer," *Symmetry*, vol. 14, no. 5, p. 980, 2022, https://doi.org/10.3390/sym14050980

[21] S. Offenbacher, B. Antony, O. Barbir, F. Auer, and M. Landgraf, "Evaluating the applicability of multi-sensor equipped tamping machines for ballast condition monitoring," *Measurement*, vol. 172, article 108881, 2021, https://doi.org/10.1016/j.measurement.2020.108881

[22] D. M. Stefanescu, "Microstructure Evolution during the Solidification of Steel," *ISIJ Int*., vol. 46, no. 6, pp. 786–794, 2006, https://doi.org/10.2355/isijinternational.46.786

[23] B. Wang, Z. G. Shi, T. L. Zhu et al. "Wear Mechanism of SiC Particles of Different Sizes on Machine Tool Guide Material GCr15," *Surface Technology*, Vol. 54, no. 1, pp. 140-149, 2025, https://doi.org/10.16490/j.cnki.issn.1001-3660.2025.01.013

[24] C. Y. Jia, Y. M. Huo, T. He, et al. "Numerical prediction of ductile damage evolution of 40CrNiMo railway axle steel during hot cross wedge rolling," *Materials Today Communications*, Vol. 33, 2022, https://doi.org/10.1016/j.mtcomm.2022.104942

[25] H. J. Pan, W. Y. Tao, L. Liu et al. "Achieving Excellent Strength–Ductility Combination by Austempering below Ms in 40CrNiMo Steels," *Advanced Engineering Materials*, Vol. 25, no. 14, 2023, https://doi.org/10.1002/adem.202300005